ACS APPLIED MATERIALS & INTERFACES

Research Article

www.acsami.org

Enhanced Performance Using an SU-8 Dielectric Interlayer in a Bulk Heterojunction Organic Solar Cell

Christina Pang,[†,‡] Vijila Chellappan,[†] Jong Hyuk Yim,[§] Mein Jin Tan,[†] Glen Tai Wei Goh,[†] Soonil Lee,[§] Jie Zhang,*[,†] and John de Mello*[,‡]

[†]Institute of Materials Research and Engineering (IMRE), Agency for Science, Technology and Research (A*STAR), 3 Research Link, 117602, Singapore

[‡]Department of Chemistry, Imperial College London, Exhibition Road, London SW7 2AZ, United Kingdom

[§]Department of Physics and Division of Energy Systems Research, Ajou University, Suwon 443-749, Korea

Supporting Information

ABSTRACT: The effect of inserting an SU-8 dielectric interlayer into inverted bulk heterojunction (BHJ) organic solar cells (OSCs) was studied. Insertion of an ultrathin layer of SU-8 between the zinc oxide (ZnO) electron transport layer and the photoactive layer resulted in a smoother interface and a 14% enhancement in power conversion efficiency. The properties of devices with and without an SU-8 interlayer were investigated using transient photovoltage (TPV) and double injection (DoI) techniques, and it was found that devices with SU-8 show longer carrier lifetimes and greater mobility–lifetime ($\mu\tau$) products than those without. Devices with SU-8 were also found to have improved stability. The results indicate that the insertion of an SU-8 interlayer reduces the recombination rate for photogenerated carriers without affecting the charge transport properties, improving overall performance and stability.

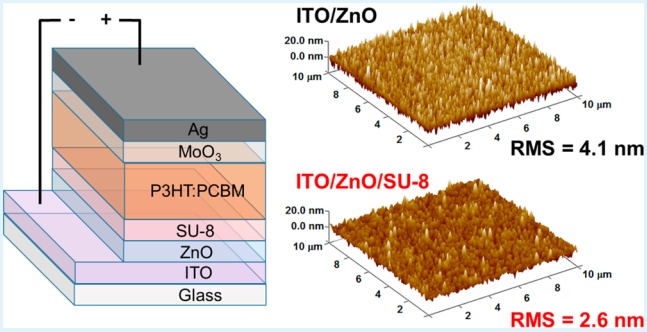

KEYWORDS: *organic solar cells, interface, insulating dielectric, electron transport layer, charge transport, ambipolar mobility, carrier lifetime, device stability*

INTRODUCTION

Organic solar cells (OSCs) have attracted much attention due to their potential for low cost, large area fabrication on flexible substrates.[1−3] The power conversion efficiencies (PCEs) of OSCs have improved significantly in recent years to more than 10%.[4] In conventional OSCs, a poly(3,4-ethylenedioxythiophene):poly(styrenesulfonate) (PEDOT:PSS) hole transporting layer is typically coated on indium tin oxide (ITO) to enhance hole collection at the anode, and a low work function metal (for example, aluminium) is typically selected as the cathode. In practice, however, the acidic PEDOT:PSS can etch the ITO, causing device degradation,[5,6] while the low work function metal oxidizes rapidly in air.

The problematic nature of PEDOT:PSS has prompted the development of alternative conducting polymer-based hole extraction layers capable of offering improved efficiency and stability.[7] An alternative and more commonly applied approach, which has the advantage of eliminating the need for both PEDOT:PSS and a (reactive) low work function cathode, is to employ an inverted device architecture.[8−10] In this case, the anode and cathode are in effect reversed by using an electron transport buffer layer in contact with the ITO, together with a high work function metal such as silver or gold as the anode. Additional interlayers are frequently used at the interfaces between the active layer and both the metal oxide and the anode to enhance efficiencies and/or device stability.[11,12]

Various metal oxides have been used for the electron transporting layer in inverted OSCs, including titanium oxide (TiO_2),[10,13] zinc oxide (ZnO),[14,15] and aluminum oxide (Al_2O_3).[16] Of these, ZnO has been most widely applied due to its high transparency, good environmental stability, low cost, and good electron transporting properties. Sol–gel processed ZnO prepared in situ from zinc acetate is frequently used for this purpose but requires high annealing temperatures of at least 250 °C for the complete removal of organic reagents and to induce crystallization.[17] As a result, it is ill-suited to flexible substrates and tandem cells where the underlying polymer layer degrades at high temperatures. To address this issue, Sun et al.[18] and Chou et al.[19] incorporated sol–gel derived ZnO films into OSCs using processing temperatures of 150 °C and below, with the resultant film comprising a mixture of ZnO and residual zinc acetate.[19] The reduced processing temperature was found to give better diode characteristics with higher

Received: November 21, 2014
Accepted: February 6, 2015
Published: February 6, 2015

DOI: 10.1021/am508177p
ACS Appl. Mater. Interfaces 2015, 7, 5219−5225

rectification ratios and reduced leakage currents.[19] However, ZnO prepared in this way is substantially rougher than that prepared by other routes,[20,21] suggesting such an approach would benefit from the use of an additional planarizing interlayer to reduce the risk of device shunting.

Conjugated polyelectrolytes (CPEs), conjugated polymers with ionic functionalities, have been reported as promising (electron-transporting) alternatives to metal oxides. When deposited on ITO, they can planarize the surface, lower the effective work function, and increase the open circuit voltage (V_{oc}) of the final device, thereby leading to improved efficiencies.[22−24] However, the stability of devices employing CPEs has not been widely reported and at least one published report has noted poorer stability compared to control devices without CPEs.[22]

Ultrathin insulating interlayers, for example, poly(4-hydroxystyrene) (PHS)[25] and poly(vinylpyrrolidone) (PVP),[26] have previously been used as cathodic interlayers in conventional (noninverted) OSCs. However, PHS, apart from offering the advantage of being solution processable, did not show any significant improvement in performance compared to lithium fluoride and calcium when inserted between the active layer and the cathode, and PVP is a hydrophilic material that may accelerate the uptake of water into the device, leading to accelerated degradation. To our knowledge, ultrathin insulating polymer layers have until now only been used as cathodic interlayers in conventional architecture devices, and they have not previously been applied to inverted architectures.

In this work, we evaluate the insulating polymer SU-8 for use as an interlayer between ZnO and the photoactive layer in inverted poly(3-hexylthiophene-2,5-diyl) (P3HT)-based devices. SU-8, a commercially available epoxy-based dielectric material (see Supporting Information Figure S1 for the chemical structure), is mechanically robust and possesses high thermal stability[27] and optical transparency at visible and near-infrared wavelengths.[28] It also has a high glass transition temperature of 200 °C and a very high degradation temperature of 380 °C.[29] Moreover, cross-linked SU-8 is highly chemical resistant, which allows additional layers to be coated on top of it without damage. These favorable properties have led to its widespread use as an insulating dielectric material in conventional microelectronics and make it an attractive candidate for use in organic devices.[30−33]

In the work reported here, we find that insertion of an SU-8 interlayer between ZnO and the active layer can reduce roughness, improve stability, and enhance efficiency by ∼15%. Charge transport and mobility studies indicate the improved efficiency is principally due to longer carrier lifetimes, i.e., a reduced rate of recombination inside the bulk of the device.

EXPERIMENTAL SECTION

Synthesis of ZnO Sol−Gel Precursor. Synthesis of the ZnO sol−gel precursor was carried out according to the procedure of Sun et al.[18] Zinc acetate dihydrate ($Zn(CH_3COO)_2{\cdot}2H_2O$, Alfa Aesar, 98−101%) was dissolved in a mixture of ethanolamine ($NH_2CH_2CH_2OH$, Aldrich, 99.5%) and 2-methoxyethanol ($CH_3OCH_2CH_2OH$, Aldrich, 99.3%). The molar ratio of zinc acetate dihydrate to ethanolamine was kept at 1:1, with a Zn concentration of 0.5 M. The solution was stirred vigorously overnight in air (to allow the hydrolysis reaction to reach completion) and then passed through a 0.2 μm PTFE filter. The obtained precursor solution was found to be stable for several months when stored in the fridge.

Device Fabrication and Characterization. ITO-coated glass substrates were cleaned by first sonicating them in a 10% (v/v) mixture of Hellmanex III detergent (Hellma Analytics) and deionized (DI) water, followed by DI water, acetone, and isopropanol (IPA). ZnO sol−gel precursor was spin coated onto the cleaned ITO substrates, which were then heated at 150 °C for 1 h to give a film thickness of approximately 35 nm.

SU-8 2050 (Microchem) was diluted to 0.08% (w/w) using the SU-8 thinner cyclopentanone. The solution was spin coated onto ZnO in a two-step process at 500 rpm for 5 s and 1000 rpm for 45 s. The substrates were then soft baked at 65 °C for 1 min and at 95 °C for 2 min to evaporate the solvent and densify the film.

To cross-link the SU-8 and render the layer insoluble during subsequent deposition of the active layer, the sample was exposed to 365 nm UV irradiation for 45 s, baked at 65 °C for 1 min and at 95 °C for 2 min, and then hard baked at 150 °C for 5 min. Uncoated layers of ZnO were also subjected to the same baking and UV irradiation steps for the fabrication of SU-8-free control devices.

The substrates were transferred to a nitrogen (N_2)-filled glovebox. A 1:0.8 blend by weight of P3HT (Rieke Metals Inc.) and [6,6]-phenyl-C61-butyric acid methyl ester ($PC_{60}BM$, Nano-C) was prepared in 1,2-dichlorobenzene (50 mg/mL) and spin-coated at 1000 rpm for 120 s to obtain a ∼200 nm film. The coated substrates were annealed in an N_2 environment at 140 °C for 10 min. Finally, the substrates were transferred to a thermal evaporator, where 10 nm of molybdenum trioxide (MoO_3) and 100 nm of silver were evaporated under a vacuum of 4×10^{-6} mbar through a shadow mask to complete the device. The active area defined by the overlap of anode and cathode was 9 mm^2. For the double injection (DoI) experiments, smaller but otherwise identical devices were fabricated with an active area of 2 mm^2 in order to reduce the RC time constant.

A Keithley 2400 source meter was used to measure current−voltage (J−V) characteristics in N_2 under 100 mW cm^{-2} AM 1.5G conditions with a SanEi solar simulator. Film thicknesses were determined using a Tencor 10 surface profiler. UV−vis transmittance spectra were measured using a Shimadzu UV-3101 spectrophotometer. Atomic force microscopy was carried out using a Bruker Dimension Icon Atomic Force Microscope (AFM) system. Ellipsometry was performed on a J.A. Woollam VASE ellipsometer. External quantum efficiency (EQE) measurements as a function of wavelength were obtained under short-circuit conditions using a lock-in amplifier (Stanford Research System, SR510) at a chopping frequency of 280 Hz under illumination with monochromatic light from a xenon arc lamp. Completed devices were encapsulated in a cover glass and sealed with an epoxy resin for further studies and stability tests.

Carrier Lifetime and Charge Mobility Measurement. The charge carrier lifetime was measured using transient photovoltage (TPV) spectroscopy.[34,35] Devices were connected to a high input (1 MΩ) impedance oscilloscope (Agilent Infiniium 1 GHz), and the open circuit voltage V_{oc} was measured at varying levels of white light illumination. A small perturbation on V_{oc} (ΔV_{oc} < 20 mV) was generated using a 532 nm pulsed Nd:YAG laser (pulse width <5 ns, pulse repetition rate 1 Hz). Under open-circuit conditions, the voltage decay is proportional to the decay of excess photogenerated carriers ($d\Delta V_{oc}/dt \propto d\Delta n/dt$), allowing direct measurement of the carrier lifetime.[36,37]

The charge mobility was measured by DoI, in which a square voltage pulse is applied in forward bias to inject carriers through both electrodes, with the current transient being recorded on an oscilloscope across a low impedance load of 50 Ω.[38] Under the influence of the applied electric field, the injected carriers drift through the device and recombine in the bulk. The ambipolar carrier mobility μ_a and transit time t_a are related by the equation $\mu_a = d^2/t_a U$ where d is the film thickness and U is the applied bias. The transit time t_a may in turn be determined from the time t_m at which the current derivative dj/dt reaches its maximum value using the relation $t_m = (5/6)t_a$; see ref 38 and Figure S2 in the Supporting Information. Combining the two equations, we obtain $\mu_a = 5d^2/6t_m U$.

DOI: 10.1021/am508177p
ACS Appl. Mater. Interfaces 2015, 7, 5219−5225

RESULTS AND DISCUSSION

The ITO/ZnO/SU-8/P3HT:PCBM/MoO_3/Ag inverted device architecture used in this work is shown in Figure 1a.

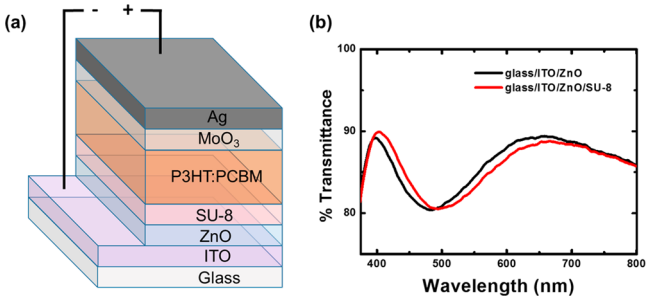

Figure 1. (a) Cell architecture of inverted devices, including SU-8 interlayer between ZnO and P3HT:PCBM. Control devices had a similar structure, except for the omission of the SU-8 layer. (b) UV–vis transmittance spectra of ZnO on ITO glass with and without a surface coating of SU-8.

Control devices had a similar structure, except for the omission of the SU-8 layer. The UV–vis transmittance spectra of glass/ITO/ZnO and glass/ITO/ZnO/SU-8 are shown in Figure 1b. High transmittances of more than 80% across the visible range were measured in both cases. The addition of SU-8 caused a slight red-shift in the transmittance spectrum but no significant change in average transmittance between 400 and 800 nm (86.0% without SU-8 vs 85.8% with). The thickness of SU-8 was determined via ellipsometry to be approximately 2.5 nm.

Figure 2 shows AFM topographic images of ITO, ITO/ZnO, and ITO/ZnO/SU-8 on glass. An increase in root-mean-square (rms) roughness from 3.5 to 4.1 nm was evident after deposition of the ZnO layer on ITO-coated glass. However, after depositing SU-8 on the ZnO, the rms roughness decreased to 2.6 nm, indicating the SU-8 layer had a beneficial planarizing effect. The extent of planarization was found to be more significant for thicker films; see Figure S3 in the Supporting Information.

The effect of the SU-8 interlayer was tested in inverted cells by fabricating P3HT:PCBM bulk heterojunction (BHJ) solar cells with and without an SU-8 interlayer (nominal thickness 2.5 nm). Figure 3 shows the current density–voltage (J–V) curves of the devices under AM 1.5G illumination and in dark conditions, with the typical photovoltaic characteristics summarized in Table 1. The shunt resistance (R_{sh}) and series resistance (R_s) were calculated from the J–V curve under illumination. Devices without an SU-8 interlayer had an average V_{oc} of 604 ± 3 mV, a fill factor (FF) of 57.6 ± 0.3%, and a short-circuit current density (J_{sc}) of 8.6 ± 0.1 mA cm^{-2}. These values correspond to a power conversion efficiency (PCE) of 2.98 ± 0.02%. Devices with an interlayer had an improved average V_{oc} of 614 ± 2 mV, an increased FF of 63.4 ± 0.2%, and a similar J_{sc} of 8.7 ± 0.1 mA cm^{-2}, corresponding to an improved PCE of 3.40 ± 0.02%.

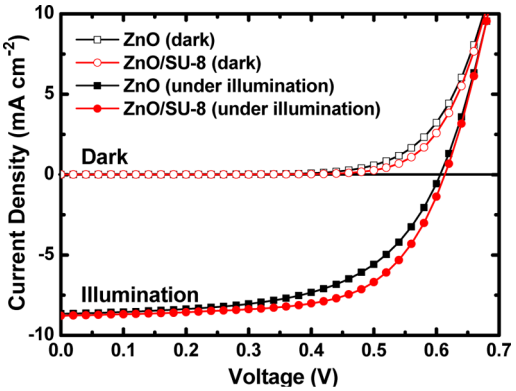

Figure 3. J–V curves of devices with and without an SU-8 interlayer in dark conditions and under AM 1.5G illumination.

The increase in FF is an indication of more efficient charge collection and a reduced rate of recombination in the SU-8-containing devices. The series resistance was not significantly affected by the inclusion of the SU-8 layer, indicating it allows charges to tunnel/flow through readily. The dark J–V curves

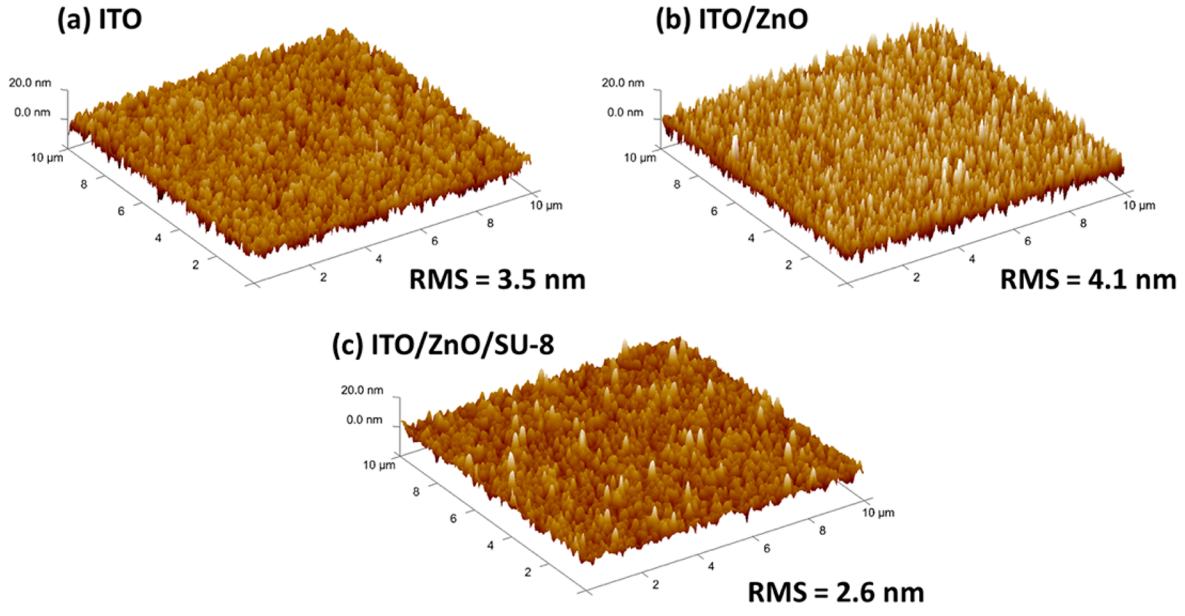

Figure 2. AFM topographic images of (a) ITO, (b) ITO/ZnO, and (c) ITO/ZnO/SU-8.

DOI: 10.1021/am508177p
ACS Appl. Mater. Interfaces 2015, 7, 5219–5225

Table 1. Characteristics of P3HT:PCBM Inverted Solar Cells with and without an SU-8 Interlayer under AM 1.5G Illumination[a]

	V_{oc} (mV)	FF (%)	J_{sc} (mA cm^{-2})	PCE (%)	shunt resistance R_{sh} (kΩ cm^2)	series resistance R_s (Ω cm^2)
ZnO	604 ± 3	57.6 ± 0.3	8.6 ± 0.1	2.98 ± 0.02	0.96 ± 0.12	2.9 ± 0.1
ZnO/SU-8	614 ± 2	63.4 ± 0.2	8.7 ± 0.1	3.40 ± 0.02	1.12 ± 0.17	2.9 ± 0.1

[a]Note: The average PCE and standard deviations were obtained from four cells.

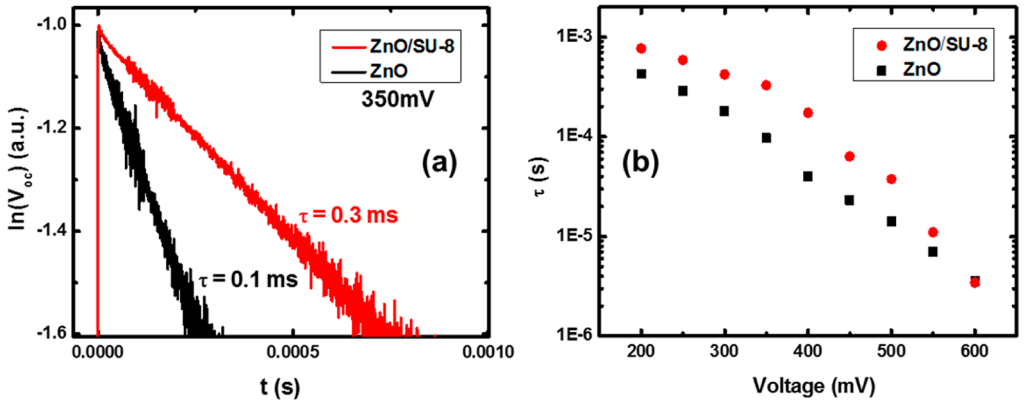

Figure 4. (a) Photovoltage decay transients recorded at 350 mV, showing a longer lifetime for devices with SU-8. (b) Carrier lifetime versus light bias determined by fitting the TPV transients to a single exponential decay.

for the two sets of devices were fairly similar, with only a slight reduction in dark current due to the SU-8 interlayer; hence, the substantial improvement in FF cannot be attributed to significantly reduced leakage in the device.

The external quantum efficiency (EQE) spectra of the devices with and without SU-8 are shown in Figure S4 in the Supporting Information. The ratio of the measured J_{sc} values agreed to within 3% with the ratio of the integrated EQE spectra. Both devices had a maximum EQE of 65% at a wavelength of 550 nm.

To investigate whether the SU-8 layer influenced the recombination dynamics in the device, carrier lifetimes τ under open-circuit conditions were extracted from TPV measurements. Figure 4a shows typical photovoltage transients for devices with and without an SU-8 interlayer under a white light reference photovoltage of 350 mV. With SU-8 present, the photovoltage decayed much more slowly, indicating slower charge recombination.

Fitting the TPV transient to a single exponential decay in Figure 4a indicated an increase in lifetime at 350 mV from 0.1 ms without SU-8 to 0.3 ms with it. The variation of τ with photovoltage is shown in Figure 4b for the two sets of devices. A progressive drop in carrier lifetime was observed in both cases: as the light bias (V_{oc}) was increased from 200 to 600 mV, the lifetime decreased from 428 to 3.6 μs in the case of the SU-8-free device and from 770 to 3.5 μs in the case of the SU-8 device. The observed reduction in carrier lifetime with increasing applied bias agrees with previous reports of TPV measurements in OSCs[34,35,39] and is in accordance with expectation: the carrier density inside the device increases at higher applied biases (since photogenerated carriers are swept toward the respective electrodes more slowly due to the reduced internal field strength), resulting in a higher rate of bimolecular recombination. Across the range of photovoltages tested, the lifetime was consistently higher for the device containing SU-8 than for the device without it, indicating a substantially reduced recombination rate at all biases up to 550 mV.

The charge carrier lifetime is not wholly responsible for determining the device performance. Instead, it is the mobility–lifetime (μ–τ) product which typically determines the distance charges travel before recombination and which therefore governs the overall efficiency.[40] The ambipolar charge carrier mobility was obtained using the DoI method and is plotted versus electric field in Figure 5 for devices with and

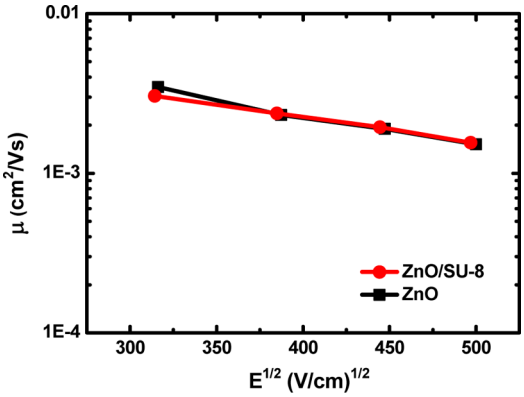

Figure 5. Ambipolar mobility versus internal field strength.

without an SU-8 interlayer. The mobilities for the two devices were very similar, varying from about 3.5×10^{-3} to 1.5×10^{-3} cm^2/(V s) as the electric field E varied from 1×10^5 to 2.5×10^5 V/cm.

It is evident from Figure 5 that the SU-8 interlayer has only a weak influence on the charge transport properties and that the improvement in device efficiency is therefore mainly attributable to the slower recombination dynamics in the SU-8 device. While further studies are required to conclusively establish the origin of the increased carrier lifetime, surface traps on the ZnO crystal are known to promote electron–hole recombination in both dye-sensitized[41] and inverted BHJ solar cells.[42] Hence, it appears likely that the SU-8 layer reduces the rate of interfacial recombination, either by reducing the rate of back electron

DOI: 10.1021/am508177p
ACS Appl. Mater. Interfaces 2015, 7, 5219–5225

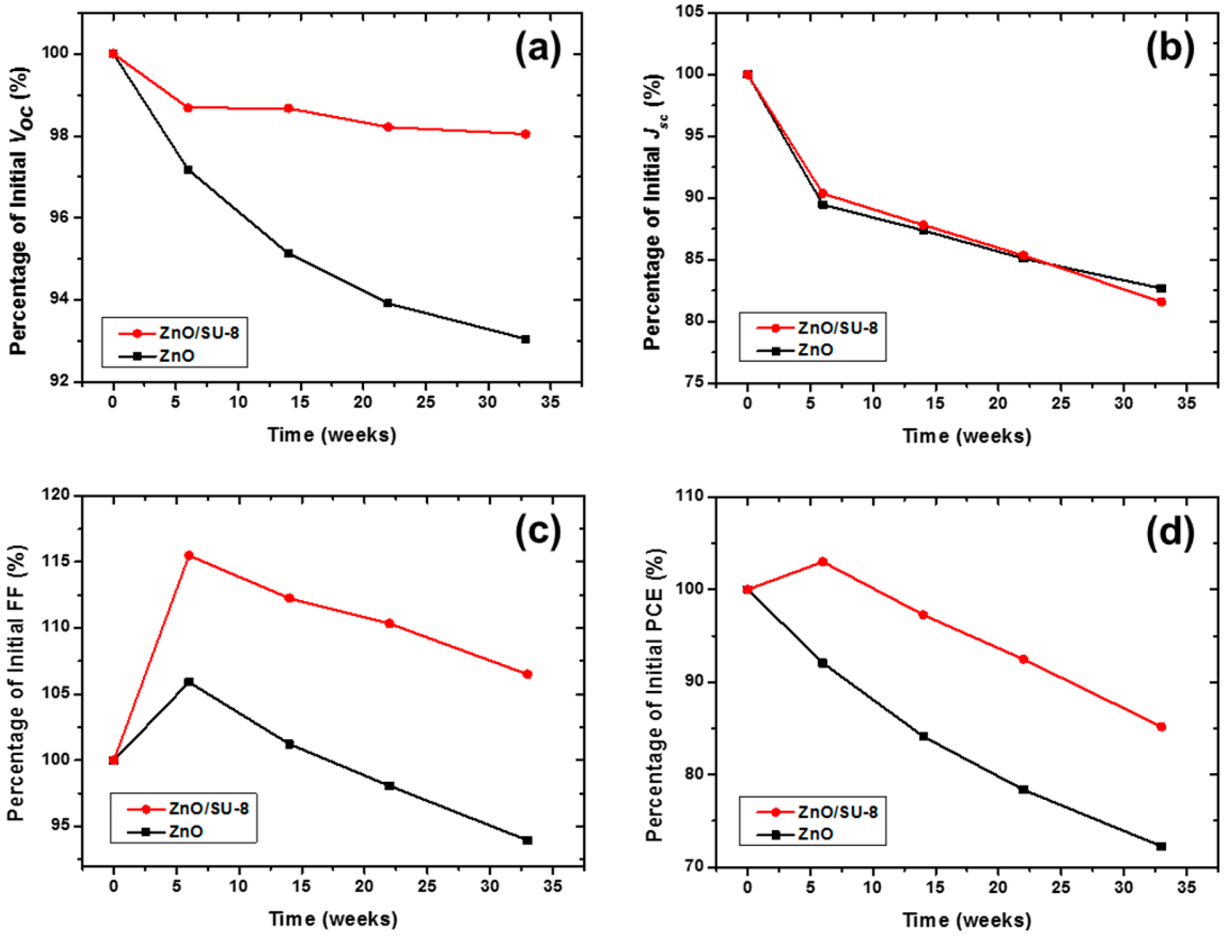

Figure 6. Normalized photovoltaic parameters of encapsulated devices with and without SU-8 versus storage time in air: (a) V_{oc}; (b) J_{sc}; (c) FF; and (d) PCE.

transfer from the metal oxide to the P3HT:PCBM active layer or by blocking holes from reaching the ZnO, thereby preventing them from coming into proximity with the trapped electrons. Both effects would lead to an increase in carrier lifetime. We note that similar effects have previously been reported using a reduced graphene-oxide/ZnO composite buffer layer.[42]

The stability in ambient conditions of encapsulated SU-8 and SU-8-free devices was investigated (see Figure 6). After 33 weeks, the SU-8 device showed a 2% drop in V_{oc} and a 6.5% increase in FF under AM 1.5G conditions, while the control device suffered a 7% reduction in V_{oc} and a 6% decrease in FF. The two devices saw a similar reduction in J_{sc}, to about 82% of the initial values. Overall, the SU-8 device retained 85% of its initial PCE after 33 weeks, while the control device retained only 72% of the initial PCE. The results suggest superior stability for devices with an SU-8 interlayer.

The reason for the improved stability requires further investigation but, upon application of a voltage or UV illumination (during testing), oxygen adsorbed on the ZnO is liable to be released into the adjacent layers.[43,44] The insertion of SU-8 between the active layer and ZnO may reduce oxygen uptake by the active layer and thereby slow down the overall rate of degradation. Also, the presence of the SU-8 may reduce the interaction of surface-trapped charges on the ZnO with the active layer and thereby inhibit any detrimental interactions with the active layer.[45]

In conclusion, the effect of coating ZnO films with an interlayer of SU-8 has been studied in inverted BHJ solar cells. The SU-8 was found to decrease the roughness of the ZnO film, improve stability, and enhance the PCE by 14%. The incorporation of an SU-8 interlayer resulted in an increased carrier lifetime but had little effect on the carrier mobility, suggesting the improved device performance is predominantly due to slower recombination dynamics in the presence of SU-8. Overall, the addition of the SU-8 interlayer was found to be beneficial in terms of both device performance and stability.

■ ASSOCIATED CONTENT

Supporting Information

Chemical structure of SU-8, DoI transient and current derivative (showing how t_m is obtained from the transient), AFM images showing surface roughness of SU-8 on ITO/ZnO for two different SU-8 thicknesses (of approximately 5.5 and 21 nm), and EQE of devices with and without an SU-8 interlayer. This material is available free of charge via the Internet at http://pubs.acs.org.

■ AUTHOR INFORMATION

Corresponding Authors

*E-mail: zhangj@imre.a-star.edu.sg.
*E-mail: j.demello@imperial.ac.uk.

Notes

The authors declare no competing financial interest.

DOI: 10.1021/am508177p
ACS Appl. Mater. Interfaces 2015, 7, 5219−5225

■ ACKNOWLEDGMENTS

This work was financially supported by A*STAR Graduate Academy and A*STAR Science Engineering Research Council's Printed Electronics Program (Grant #1021700137).

■ REFERENCES

(1) Coakley, K. M.; McGehee, M. D. Conjugated Polymer Photovoltaic Cells. *Chem. Mater.* **2004**, *16*, 4533−4542.
(2) Krebs, F. C. Fabrication and Processing of Polymer Solar Cells: A Review of Printing and Coating Techniques. *Sol. Energy Mater. Sol. C* **2009**, *93*, 394−412.
(3) Brabec, C. J.; Gowrisanker, S.; Halls, J. J. M.; Laird, D.; Jia, S.; Williams, S. P. Polymer−Fullerene Bulk-Heterojunction Solar Cells. *Adv. Mater.* **2010**, *22*, 3839−3856.
(4) You, J.; Dou, L.; Yoshimura, K.; Kato, T.; Ohya, K.; Moriarty, T.; Emery, K.; Chen, C.-C.; Gao, J.; Li, G.; Yang, Y. A Polymer Tandem Solar Cell with 10.6% Power Conversion Efficiency. *Nat. Commun.* **2013**, *4*, 1446-1−1446-10.
(5) de Jong, M. P.; van Ijzendoorn, L. J.; de Voigt, M. J. A. Stability of the Interface between Indium-Tin-Oxide and Poly(3,4-Ethylenedioxythiophene)/Poly(Styrenesulfonate) in Polymer Light-Emitting Diodes. *Appl. Phys. Lett.* **2000**, *77*, 2255−2257.
(6) Norrman, K.; Madsen, M. V.; Gevorgyan, S. A.; Krebs, F. C. Degradation Patterns in Water and Oxygen of an Inverted Polymer Solar Cell. *J. Am. Chem. Soc.* **2010**, *132*, 16883−16892.
(7) Choi, M.-R.; Han, T.-H.; Lim, K.-G.; Woo, S.-H.; Huh, D. H.; Lee, T.-W. Soluble Self-Doped Conducting Polymer Compositions with Tunable Work Function as Hole Injection/Extraction Layers in Organic Optoelectronics. *Angew. Chem., Int. Ed.* **2011**, *50*, 6274−6277.
(8) Zhao, D. W.; Liu, P.; Sun, X. W.; Tan, S. T.; Ke, L.; Kyaw, A. K. K. An Inverted Organic Solar Cell with an Ultrathin Ca Electron-Transporting Layer and MoO3 Hole-Transporting Layer. *Appl. Phys. Lett.* **2009**, *95*, 153304-1−153304-3.
(9) Steim, R.; Choulis, S. A.; Schilinsky, P.; Brabec, C. J. Interface Modification for Highly Efficient Organic Photovoltaics. *Appl. Phys. Lett.* **2008**, *92*, 093303-1−093303-3.
(10) Waldauf, C.; Morana, M.; Denk, P.; Schilinsky, P.; Coakley, K.; Choulis, S. A.; Brabec, C. J. Highly Efficient Inverted Organic Photovoltaics Using Solution Based Titanium Oxide as Electron Selective Contact. *Appl. Phys. Lett.* **2006**, *89*, 233517-1−233517-3.
(11) Park, J. H.; Lee, T.-W.; Chin, B.-D.; Wang, D. H.; Park, O. O. Roles of Interlayers in Efficient Organic Photovoltaic Devices. *Macromol. Rapid Commun.* **2010**, *31*, 2095−2108.
(12) Lee, T.-W.; Lim, K.-G.; Kim, D.-H. Approaches toward Efficient and Stable Electron Extraction Contact in Organic Photovoltaic Cells: Inspiration from Organic Light-Emitting Diodes. *Electron. Mater. Lett.* **2010**, *6*, 41−50.
(13) Hau, S. K.; Yip, H.-L.; Acton, O.; Baek, N. S.; Ma, H.; Jen, A. K. Y. Interfacial Modification to Improve Inverted Polymer Solar Cells. *J. Mater. Chem.* **2008**, *18*, 5113−5119.
(14) Kyaw, A. K. K.; Sun, X. W.; Jiang, C. Y.; Lo, G. Q.; Zhao, D. W.; Kwong, D. L. An Inverted Organic Solar Cell Employing a Sol-Gel Derived ZnO Electron Selective Layer and Thermal Evaporated MoO3 Hole Selective Layer. *Appl. Phys. Lett.* **2008**, *93*, 221107-1−221107-3.
(15) White, M. S.; Olson, D. C.; Shaheen, S. E.; Kopidakis, N.; Ginley, D. S. Inverted Bulk-Heterojunction Organic Photovoltaic Device Using a Solution-Derived ZnO Underlayer. *Appl. Phys. Lett.* **2006**, *89*, 143517-1−143517-3.
(16) Zhou, Y.; Cheun, H.; Potscavage, J. W. J.; Fuentes-Hernandez, C.; Kim, S.-J.; Kippelen, B. Inverted Organic Solar Cells with ITO Electrodes Modified with an Ultrathin Al_2O_3 Buffer Layer Deposited by Atomic Layer Deposition. *J. Mater. Chem.* **2010**, *20*, 6189−6194.
(17) Kim, Y.-S.; Tai, W.-P.; Shu, S.-J. Effect of Preheating Temperature on Structural and Optical Properties of ZnO Thin Films by Sol−Gel Process. *Thin Solid Films* **2005**, *491*, 153−160.
(18) Sun, Y.; Seo, J. H.; Takacs, C. J.; Seifter, J.; Heeger, A. J. Inverted Polymer Solar Cells Integrated with a Low-Temperature-Annealed Sol-Gel-Derived ZnO Film as an Electron Transport Layer. *Adv. Mater.* **2011**, *23*, 1679−1683.
(19) Chou, C.-H.; Kwan, W. L.; Hong, Z.; Chen, L.-M.; Yang, Y. A Metal-Oxide Interconnection Layer for Polymer Tandem Solar Cells with an Inverted Architecture. *Adv. Mater.* **2011**, *23*, 1282−1286.
(20) Jun, T.; Song, K.; Jeong, Y.; Woo, K.; Kim, D.; Bae, C.; Moon, J. High-Performance Low-Temperature Solution-Processable ZnO Thin Film Transistors by Microwave-Assisted Annealing. *J. Mater. Chem.* **2011**, *21*, 1102−1108.
(21) Gieraltowska, S.; Wachnicki, L.; Witkowski, B. S.; Godlewski, M.; Guziewicz, E. Atomic Layer Deposition Grown Composite Dielectric Oxides and ZnO for Transparent Electronic Applications. *Thin Solid Films* **2012**, *520*, 4694−4697.
(22) Chang, Y.-M.; Leu, C.-Y. Conjugated Polyelectrolyte and Zinc Oxide Stacked Structure as an Interlayer in Highly Efficient and Stable Organic Photovoltaic Cells. *J. Mater. Chem. A* **2013**, *1*, 6446−6451.
(23) He, Z.; Zhong, C.; Su, S.; Xu, M.; Wu, H.; Cao, Y. Enhanced Power-Conversion Efficiency in Polymer Solar Cells Using an Inverted Device Structure. *Nat. Photonics* **2012**, *6*, 591−595.
(24) Yang, T.; Wang, M.; Duan, C.; Hu, X.; Huang, L.; Peng, J.; Huang, F.; Gong, X. Inverted Polymer Solar Cells with 8.4% Efficiency by Conjugated Polyelectrolyte. *Energy Environ. Sci.* **2012**, *5*, 8208−8214.
(25) Lim, K.-G.; Choi, M.-R.; Kim, H.-B.; Park, J. H.; Lee, T.-W. High-Efficiency Polymer Photovoltaic Cells Using a Solution-Processable Insulating Interfacial Nanolayer: The Role of the Insulating Nanolayer. *J. Mater. Chem.* **2012**, *22*, 25148−25153.
(26) Wang, H.; Zhang, W.; Xu, C.; Bi, X.; Chen, B.; Yang, S. Efficiency Enhancement of Polymer Solar Cells by Applying Poly(vinylpyrrolidone) as a Cathode Buffer Layer Via Spin Coating or Self-Assembly. *ACS Appl. Mater. Interfaces* **2012**, *5*, 26−34.
(27) Lorenz, H.; Despont, M.; Fahrni, N.; LaBianca, N.; Renaud, P.; Vettiger, P. SU-8: A Low-Cost Negative Resist for MEMS. *J. Micromech. Microeng.* **1997**, *7*, 121−124.
(28) Lee, K. Y.; LaBianca, N.; Rishton, S. A.; Zolgharnain, S.; Gelorme, J. D.; Shaw, J.; Chang, T. H. P. Micromachining Applications of a High Resolution Ultrathick Photoresist. *J. Vac. Sci. Technol., B* **1995**, *13*, 3012−3016.
(29) del Campo, A.; Greiner, C. SU-8: A Photoresist for High-Aspect-Ratio and 3D Submicron Lithography. *J. Micromech. Microeng.* **2007**, *17*, R81−R95.
(30) Lee, K. J.; Motala, M. J.; Meitl, M. A.; Childs, W. R.; Menard, E.; Shim, A. K.; Rogers, J. A.; Nuzzo, R. G. Large-Area, Selective Transfer of Microstructured Silicon: A Printing-Based Approach to High-Performance Thin-Film Transistors Supported on Flexible Substrates. *Adv. Mater.* **2005**, *17*, 2332−2336.
(31) Menard, E.; Lee, K. J.; Khang, D.-Y.; Nuzzo, R. G.; Rogers, J. A. A Printable Form of Silicon for High Performance Thin Film Transistors on Plastic Substrates. *Appl. Phys. Lett.* **2004**, *84*, 5398−5400.
(32) Yuan, H.-C.; Ma, Z.; Roberts, M. M.; Savage, D. E.; Lagally, M. G. High-Speed Strained-Single-Crystal-Silicon Thin-Film Transistors on Flexible Polymers. *J. Appl. Phys.* **2006**, *100*, 013708-1−013708-5.
(33) Zhou, K.; Heikenfeld, J.; Dean, K. A.; Howard, E. M.; Johnson, M. R. A Full Description of a Simple and Scalable Fabrication Process for Electrowetting Displays. *J. Micromech. Microeng.* **2009**, *19*, 065029-1−065029-12.
(34) Shuttle, C. G.; O'Regan, B.; Ballantyne, A. M.; Nelson, J.; Bradley, D. D. C.; de Mello, J.; Durrant, J. R. Experimental Determination of the Rate Law for Charge Carrier Decay in a Polythiophene: Fullerene Solar Cell. *Appl. Phys. Lett.* **2008**, *92*, 093311-1−093311-3.
(35) Elumalai, N. K.; Jin, T. M.; Chellappan, V.; Jose, R.; Palaniswamy, S. K.; Jayaraman, S.; Raut, H. K.; Ramakrishna, S. Electrospun ZnO Nanowire Plantations in the Electron Transport Layer for High-Efficiency Inverted Organic Solar Cells. *ACS Appl. Mater. Interfaces* **2013**, *5*, 9396−9404.
(36) Bisquert, J.; Fabregat-Santiago, F.; Mora-Seró, I.; Garcia-Belmonte, G.; Giménez, S. Electron Lifetime in Dye-Sensitized Solar

DOI: 10.1021/am508177p
ACS Appl. Mater. Interfaces 2015, 7, 5219−5225

Cells: Theory and Interpretation of Measurements. *J. Phys. Chem. C* **2009**, *113*, 17278−17290.
(37) Ajuria, J.; Etxebarria, I.; Azaceta, E.; Tena-Zaera, R.; Fernandez-Montcada, N.; Palomares, E.; Pacios, R. Novel ZnO Nanostructured Electrodes for Higher Power Conversion Efficiencies in Polymeric Solar Cells. *Phys. Chem. Chem. Phys.* **2011**, *13*, 20871−20876.
(38) Juska, G.; Arlauskas, K.; Sliauzys, G.; Pivrikas, A.; Mozer, A. J.; Sariciftci, N. S.; Scharber, M.; Osterbacka, R. Double Injection as a Technique to Study Charge Carrier Transport and Recombination in Bulk-Heterojunction Solar Cells. *Appl. Phys. Lett.* **2005**, *87*, 222110-1−222110-3.
(39) Foertig, A.; Rauh, J.; Dyakonov, V.; Deibel, C. Shockley Equation Parameters of P3HT:PCBM Solar Cells Determined by Transient Techniques. *Phys. Rev. B* **2012**, *86*, 115302-1−115302-7.
(40) Pivrikas, A.; Sariciftci, N. S.; Juška, G.; Österbacka, R. A Review of Charge Transport and Recombination in Polymer/Fullerene Organic Solar Cells. *Prog. Photovoltaics: Res. Appl.* **2007**, *15*, 677−696.
(41) Etgar, L.; Bendall, J. S.; Laporte, V.; Welland, M. E.; Graetzel, M. Reducing Recombination in ZnO Photoanodes for Dye Sensitised Solar Cells through Simple Chemical Synthesis. *J. Mater. Chem.* **2012**, *22*, 24463−24468.
(42) Lee, H. W.; Oh, J. Y.; Lee, T. I.; Jang, W. S.; Yoo, Y. B.; Chae, S. S.; Park, J. H.; Myoung, J. M.; Song, K. M.; Baik, H. K. Highly Efficient Inverted Polymer Solar Cells with Reduced Graphene-Oxide-Zinc-Oxide Nanocomposites Buffer Layer. *Appl. Phys. Lett.* **2013**, *102*, 193903-1−193903-4.
(43) Krebs, F. C.; Tromholt, T.; Jorgensen, M. Upscaling of Polymer Solar Cell Fabrication Using Full Roll-to-Roll Processing. *Nanoscale* **2010**, *2*, 873−886.
(44) Verbakel, F.; Meskers, S. C. J.; Janssen, R. A. J. Electronic Memory Effects in Diodes from a Zinc Oxide Nanoparticle-Polystyrene Hybrid Material. *Appl. Phys. Lett.* **2006**, *89*, 102103-1−102103-3.
(45) Hsieh, C.-H.; Cheng, Y.-J.; Li, P.-J.; Chen, C.-H.; Dubosc, M.; Liang, R.-M.; Hsu, C.-S. Highly Efficient and Stable Inverted Polymer Solar Cells Integrated with a Cross-Linked Fullerene Material as an Interlayer. *J. Am. Chem. Soc.* **2010**, *132*, 4887−4893.

DOI: 10.1021/am508177p
ACS Appl. Mater. Interfaces 2015, 7, 5219−5225